

Hidden physics in the dual-fermion approach - a special case of a non-local expansion scheme

Gang Li^{1,*}

¹*Institut für Theoretische Physik und Astrophysik, Universität Würzburg, 97074 Würzburg, Germany*

In this work, we present a non-local expansion scheme to study correlated electron systems aiming at a better description of its spatial fluctuations at all length scales. Taking the non-local coupling as a perturbation to the local degrees of freedom, we show that the non-locality in the self-energy function can be efficiently constructed from the coupling between local fluctuations. It can provide one unified framework to incorporate non-locality to both ordered and disordered correlated many-body fermion systems. As the first application, we prove that the dual-fermion approach can be understood as a special case of this non-local expansion scheme. The scheme presented in this work is constructed without introducing any dual variable, in which the interacting nature and the correlated behaviors of the lattice fermions have a clear physics correspondence. Thus, in this special case, the equivalence of the dual-fermion approach to the non-local expansion scheme beautifully reveals the physics origin of the dual variables. We show that the non-interacting dual-fermion Green's function corresponds exactly to a non-local coupling of the lattice fermion renormalized by the local single-particle charge fluctuations, and the dual-fermion self-energy behaves as the one-particle fully irreducible components of the lattice Green's function. Not only limited to this specific example, the non-local expansion scheme presented in this work can also be applied to other problems depending on the choice of the local degrees of freedom.

PACS numbers: 71.10.Fd, 71.27.+a, 71.30.+h

I. INTRODUCTION

The Bloch's theorem [1] for electron states in crystals is based on their translational symmetry. These states are labeled by the quantum number k , which reflects their invariant behaviours under a translation by a Bravais lattice vector. However, the translational symmetry in a real solid is never perfect, which is not only because of its finite dimension, but also because of the presence of chemical potential/interaction disorders, lattice defects, impurities and phonons, etc. The finite dimension of a system may give rise to states which are sensitive to the surface but insensitive to the interior of the bulk. The chemical potential or interaction disorder localizes electron states in real space which can trigger a metal-insulator transition (also known as an Anderson transition [2]). In the ultracold atom system in optical lattices [3], though the lattice defects, impurities or phonons are absent, the spatial inhomogeneity is always present, as harmonic confinement potential introduces a spatially varying local density, which breaks translational symmetry of these cold atom systems. In addition, in systems with short-ranged magnetic correlations, the homogeneity can also be broken by the creation of ordered patterns in real space. When the concentration of disorder or magnetic patterns is small, the system can be treated approximatedly as if the translational symmetry were not broken, in this case the quantum number k can still be used to characterize the electron states. However, in the case with strong disorders, the translational symmetry

should be completely abandoned. Thus, it is important to have a unified theoretical framework to capture the effects of spatial inhomogeneity, especially in the presence of strong electronic correlations.

This problem represents a strong challenge to modern many-body theories. Due to the presence of the strong electronic correlation, approaches formulated from either weak-coupling or strong-coupling expansions, such as fluctuation exchange (FLEX) [4], random phase approximation (RPA), cumulant expansion [5, 6], strong-coupling expansion [7, 8], etc. are not adequate to handle the complete parameter range in interaction. Unbiased numerical approaches, such as exact-diagonalization and quantum Monte Carlo [9, 10], can treat the correlation effect precisely, but with the penalty on their finite cluster size, *i.e.* the thermodynamic limit is not directly available in these approaches. Another class of many-body approaches, based on the dynamical mean-field theory (DMFT) [11], can fairly treat electronic correlation at arbitrary strength and contain the thermodynamic limit from their construction. It has been shown that, the DMFT can provide very important insights for several nonperturbative properties, such as the Mott-Hubbard transition. It also shows its great power in the study of correlated inhomogeneous systems. In the so-called real-space DMFT (R-DMFT) [12, 13], the correlated and disordered sites are treated as a group of Anderson impurities, which are embedded into a lattice system at the thermodynamic limit via the DMFT self-consistency. However, the DMFT is exact only in the infinite spatial dimension limit, where the character of correlation effects is purely local in space. For realistic systems at finite dimension, the DMFT downgrades to an approximation, which neglects the spatial fluctu-

* Correspondence and requests for materials should be addressed to: gangli@physik.uni-wuerzburg.de

ation effect beyond the mean-field level. For this reason, in the R-DMFT, disorder and correlation effect is treated locally. The spatial fluctuations of the complete system are determined by the coupling of the impurities within strong-coupling perturbation theory at leading order only (mean-field level). Generalizing an impurity to a cluster incorporates the short-ranged spatial fluctuations inside the cluster. Both, a reciprocal-space (dynamical cluster approximation, DCA [14–18]) and a real-space construction (cellular dynamical mean field theory, Cellular-DMFT [19, 20]) have been suggested. These approaches improve results for $D = 1, 2, 3$, while the longer-ranged spatial fluctuations beyond the mean-field level are still missing. Alternative to the cluster extensions of the DMFT, the non-local fluctuations can also be restored by the so-called “diagrammatic expansion” methods. These methods include the “advanced” fluctuation-exchange scheme [21], dynamical vertex approximation (DFA) [22, 23], the dual-fermion (DF) approach [24–26] and the one-particle irreducible functional approach [27]. The non-locality in these methods is constructed from the dynamical scattering of multiple particles at the same spatial location. Comparing to the cluster extensions of the DMFT, it can be shown that both short- and long-range fluctuations are equally treated in these methods. The DFA and the DF can also be easily adapted to the study of inhomogeneous systems [28, 29] and shows their advantage over the R-DMFT.

In this paper, in line with all other “diagrammatic expansion” methods, we consider a correlated system without translational symmetry and aim at a better description of the spatial fluctuations at all length scales in the presence of strong electron-electron interaction. To this purpose, we generalize the strong-coupling expansion approach (cumulant expansion) to such a system and treat the non-local coupling as perturbations. The expansion of the non-local coupling can generate, order by order, the non-local spatial fluctuations from the coupling of the local charge fluctuations at different spatial locations. Compared to the other “diagrammatic expansion” methods mentioned above, the derivation of this scheme is rather general and the choice of the local system is quite flexible, which may provide valuable insights and understanding into other methods. For example, as will be shown in this paper, the DF approach can be understood as one special case of this non-local expansion scheme. Furthermore, depending on the choice of the local system, this scheme can either nicely go beyond the R-DMFT approximation to result in a non-local self-energy for correlated disordered systems or provide a quick cluster solver for the Cellular-DMFT. Not limited to these two specific applications, our scheme provides one unified framework to incorporate non-locality to a correlated many-body system with only moderate numerical cost.

II. NON-LOCAL EXPANSION

The translational symmetry of a homogeneous correlated system can be broken, for example, by disorders in chemical potential or interactions. But inhomogeneity in a real system can be much more general and have many different origins. The only assumption we make in this work is that the interaction shall be local. An example Hamiltonian looks like the following,

$$H = - \sum_{i,j} (c_{i\sigma}^\dagger \mathbf{t}_{i,j} c_{j\sigma} + h.c.) - \sum_i \mu_i n_i + \sum_i U_i n_{i\uparrow} n_{i\downarrow}. \quad (1)$$

Here, the values of the chemical potential μ_i and the Coulomb repulsion U_i depend on their spatial coordinations, their different values in space give rise to the spatial inhomogeneity. $\mathbf{t}_{i,j}$, in this equation, does not have to be restricted to only nearest neighbors. It can be quite general to contain more hopping terms, or spatial anisotropy, etc. Eq. (1) represents one type of inhomogeneity that the systems could have. As we discussed before, there are many other ways to induce disorders to the systems. Not losing generality, we discard the specific form of the Hamiltonian and only cast it into two parts for the convenience of the following discussions.

$$H = \sum_{i=1}^N H_i + H^{NL}. \quad (2)$$

H_i gathers every term that is locally related to site i . All other terms that carry non-locality are grouped into H^{NL} . The corresponding action can be written as

$$\begin{aligned} \mathcal{S} &= \int d\tau d\tau' \sum_{i,j} c_{i\sigma}^*(\tau) [\mathcal{G}^{-1}(\tau - \tau')]_{i,j} c_{j\sigma}(\tau') \\ &\quad + \sum_i \int d\tau U_i n_{i\uparrow}(\tau) n_{i\downarrow}(\tau) \\ &= \sum_{i=1}^N \mathcal{S}_i + \int d\tau d\tau' \sum_{i \neq j} c_{i\sigma}^*(\tau) [\mathcal{G}_\sigma^{-1}(\tau - \tau')]_{i,j} c_{j\sigma}(\tau') \\ &= \sum_{i=1}^N \mathcal{S}_i + T \sum_{i \neq j} \sum_{\omega} c_{i\omega\sigma}^* [\mathcal{G}_\sigma^{-1}(\omega)]_{i,j} c_{j\omega\sigma} \end{aligned} \quad (3)$$

where $[\mathcal{G}(\omega)_\sigma^{-1}]_{i,j}$ describes the dynamic coupling between states at different spacial locations. \mathcal{S}_i is the action that contains only the local degrees of freedom, in which $[\mathcal{G}_\sigma^{-1}(\omega)]_{ii}$ can have many different forms. For example, in the cellular-DMFT, $[\mathcal{G}(\omega)_\sigma^{-1}]_{ii} = -(\omega + \mu) + \Delta_{ii}(\omega)$, which is the local component of the inverse Weiss field. $[\mathcal{G}(\omega)_\sigma^{-1}]_{i \neq j}$ is the non-local hybridization function $\Delta_{i \neq j}(\omega)$. There are also many other possibilities of $[\mathcal{G}(\omega)_\sigma^{-1}]_{i \neq j}$. For the moment we keep $[\mathcal{G}(\omega)_\sigma^{-1}]_{i \neq j}$ as a general function that is purely non-local in space. At the end of this section, we will examine some specific forms of $[\mathcal{G}(\omega)_\sigma^{-1}]_{i,j}$ to show that, actually, the formalism presented in this work can be nicely linked to some

widely-known powerful methods, especially it can extend these local many-body approaches to partially include non-trivial spatial fluctuations. To be more precise, we refer the non-trivial spatial fluctuations to the spatial dependence in the self-energy function. If self-energy is purely a local function, the corresponding spatial fluctuations are trivial.

A. diagram expansion

The general idea of the non-local expansion approach is very simple: we take the second term on the r.h.s.

$$\begin{aligned} G_{\alpha\beta}^{\omega} &= -\langle c_{\alpha\omega} c_{\beta\omega}^* \rangle = -\frac{1}{\mathcal{Z}} \int \mathcal{D}[c^*, c] \exp \left[-\sum_{i=1}^N \mathcal{S}[c_i^*, c_i] - T \sum_{i \neq j} \sum_{\omega'} c_{i\omega'}^* V_{ij}^{\omega'} c_{j\omega'} \right] c_{\alpha\omega} c_{\beta\omega}^* \\ &= -\frac{1}{\mathcal{Z}} \prod_{i=1}^N \int \mathcal{D}[c_i^*, c_i] e^{-\mathcal{S}_i[c_i^*, c_i]} \sum_{n=0}^{\infty} \frac{(-T)^n}{n!} \left[\sum_{i \neq j} \sum_{\omega'} c_{i\omega'}^* V_{ij}^{\omega'} c_{j\omega'} \right]^n c_{\alpha\omega} c_{\beta\omega}^*. \end{aligned} \quad (4)$$

Here, α, β are two arbitrary spatial indices. \mathcal{Z} is the full partition function containing both local and non-local contributions.

$$\mathcal{Z} = \int \mathcal{D}[c^*, c] \exp \left[-\sum_{i=1}^N \mathcal{S}_i[c_i^*, c_i] - T \sum_{i \neq j} \sum_{\omega'} c_{i\omega'}^* V_{ij}^{\omega'} c_{j\omega'} \right]. \quad (5)$$

\mathcal{Z} can be replaced by the local partition function $\mathcal{Z}_{loc} = \prod_{i=1}^N \mathcal{Z}_i$ when only the connected diagrams are considered in Eq. (4), as we will do in this work. In a calculation with only the local \mathcal{S}_i , the single-particle Green's function one can get is the one with $\alpha = \beta$,

$$g_{\alpha}^{\omega} = -\prod_{i=1}^N \frac{1}{\mathcal{Z}_i} \int \mathcal{D}[c_i^*, c_i] \exp [-\mathcal{S}_i[c_i^*, c_i]] c_{\alpha\omega} c_{\alpha\omega}^*. \quad (6)$$

All terms for $\alpha \neq \beta$ vanish as the two operators, $c_{\omega\alpha}$ and $c_{\omega\beta}^*$, must pair in the above grassmann integral. With this in mind, we will proceed to evaluate the expansion in Eq. (4) order by order. Before proceeding, we want to note that Eq. (4) was more often evaluated by introducing a dual variable from the Hubbard-Stratonovich transformation [30, 31] on the non-local term. Here, we want to keep the present form of Eq. (4) and do not introduce any dual variable. At the end of this paper, we will compare our formalism to those obtained from the Hubbard-Stratonovich transformation to illuminate the physics hidden behind the introduction of the dual variables in those approaches.

of Eq. (3) as a perturbation to the local action \mathcal{S}_i . By expanding this term, we will be able to determine the non-local dynamic quantity, such as the single-particle Green's function, from the local action \mathcal{S}_i . For simplicity, we take $[\mathcal{G}(\omega)_{\sigma}^{-1}]_{ij}$ as V_{ij}^{ω} and $\omega \equiv (\omega, \sigma)$. With Eq. (3), the single-particle Green's function is calculated as

The first term in the expansion of Eq. (4) is exactly the local Green's function as defined in Eq. (6). In the second term, α and β must be different as $i \neq j$. The only way to pair these operators is to set $i = \alpha$ and $\beta = j$, which gives rise to the first *non-local* correction to \mathcal{S}_i ,

$$G_{\alpha \neq \beta}^{\omega, (a)} = g_{\alpha}^{\omega} V_{\alpha\beta}^{\omega} g_{\beta}^{\omega}. \quad (7)$$

The graphical representation of this term is shown in Fig. 1(a). The wiggly line represents the non-local hybridization $V_{\alpha\beta}$ between the two spatial locations α and β . The solid line circling at each location represents the local Green's function computed from \mathcal{S}_i , as given in Eq. (6).

The third expansion term in Eq. (4) contains two topologically distinct diagrams. They correspond to the corrections of the non-local charge fluctuations to the local and non-local Green's functions, respectively. When $\alpha = \beta$, this term gives the first correction to the local Green's function g_{α}^{ω} , which is generated from the non-local charge fluctuations coupled with the local two-particle vertex. To see this, we need to examine the possible contractions of operators connecting to $c_{\alpha\omega} c_{\alpha\omega}^*$. In order to have a connected diagram, one has to link either $c_{j\omega'} c_{k\omega''}^*$ or $c_{i\omega'}^* c_{l\omega''}$ to $c_{\alpha\omega} c_{\alpha\omega}^*$ with the corresponding constraint $j = k = \alpha$ or $i = l = \alpha$. We notice that the interchange of indices i, j with k, l does not generate topologically new diagrams, thus, we can focus on only one of them and neglect the factor $1/2$, e.g. $j = k = \alpha$.

$$\begin{aligned}
G_{\alpha=\beta}^{\omega,(b)} &= \frac{T^2}{Z_{loc}} \sum_{i \neq j} \sum_{k \neq l} \sum_{\omega', \omega''} \int \mathcal{D}[c^*, c] e^{-S_{loc}[c^*, c]} c_{l\omega''} c_{i\omega'}^* V_{i,j}^{\omega'} V_{k,l}^{\omega''} c_{j\omega'} c_{k\omega''}^* c_{\alpha\omega} c_{\alpha\omega}^* \delta_{\omega', \omega''} \delta_{i,l} \delta_{j,k} \\
&= T \sum_i \sum_{\omega'} \langle c_{i\omega'} c_{i\omega'}^* \rangle V_{i,\alpha}^{\omega'} V_{\alpha,i}^{\omega''} \langle c_{\alpha\omega'} c_{\alpha\omega'}^* c_{\alpha\omega''} c_{\alpha\omega''}^* \rangle \delta_{\omega', \omega''}.
\end{aligned} \tag{8}$$

The last term in the above equation is the local four-point correlation function computed from \mathcal{S}_i .

$$\langle c_{\alpha\omega'} c_{\alpha\omega''}^* c_{\alpha\omega} c_{\alpha\omega}^* \rangle = \langle c_{\alpha\omega'} c_{\alpha\omega''}^* c_{\alpha\omega} c_{\alpha\omega}^* \rangle_c + \langle c_{\alpha\omega'} c_{\alpha\omega''}^* \rangle \langle c_{\alpha\omega} c_{\alpha\omega}^* \rangle - \langle c_{\alpha\omega'} c_{\alpha\omega}^* \rangle \langle c_{\alpha\omega''} c_{\alpha\omega''}^* \rangle, \tag{9}$$

which contains both connected and disconnected parts. Eq. (8) corresponds to Fig. 1(b) if the connected four-point correlation function is used. The connected four-point correlation function $\langle c_{\alpha\omega'} c_{\alpha\omega''}^* c_{\alpha\omega} c_{\alpha\omega}^* \rangle_c$ (after decided by four single-particle Green's function) is also called the complete two-particle vertex, which is graphically represented as the square in Fig. 1(b).

The disconnected part of $\langle c_{\alpha\omega'} c_{\alpha\omega''}^* c_{\alpha\omega} c_{\alpha\omega}^* \rangle$ gives rise to a diagram topologically equivalent to Fig. 1(c) but with $\alpha = \beta$. This is easier to see by first assuming $\alpha \neq \beta$ in the third order expansion, and releasing this constraint at the end of the discussion,

$$\begin{aligned}
G_{\alpha \neq \beta}^{\omega,(c)} &= -\frac{T^2}{Z_{loc}} \sum_{i \neq j} \sum_{k \neq l} \sum_{\omega', \omega''} \int \mathcal{D}[c^*, c] e^{-S_{loc}[c^*, c]} c_{\alpha\omega} c_{i\omega'}^* V_{i,j}^{\omega'} V_{k,l}^{\omega''} c_{j\omega'} c_{k\omega''}^* c_{l\omega''} c_{\beta\omega}^* \\
&= -\sum_j \langle c_{\alpha\omega'} c_{i\omega'}^* \rangle V_{i,j}^{\omega'} V_{k,l}^{\omega''} \langle c_{j\omega'} c_{k\omega''}^* \rangle \langle c_{l\omega''} c_{\beta\omega}^* \rangle \delta_{i,\alpha} \delta_{j,k} \delta_{l,\beta} \delta_{\omega,\omega'} \delta_{\omega', \omega''} = g_{\alpha}^{\omega} \left(\sum_j V_{\alpha,j}^{\omega} g_j^{\omega} V_{j,\beta}^{\omega} \right) g_{\beta}^{\omega}.
\end{aligned} \tag{10}$$

Similar to Fig. 1(a), this diagram consists of only local single-particle charge fluctuations at different spatial locations which are connected by their dynamic hybridization. There will be more similar diagrams in the higher order expansions of Eq. (4). These terms can be cast into a more compact form by renormalizing the hybridization as shown in Fig. 1(d). The dressed hybridization is simply found to be

$$\tilde{V}_{\alpha\beta} = [V^{-1} - g\mathbb{1}]_{\alpha\beta}^{-1}, \tag{11}$$

where $\mathbb{1}$ is an unit matrix. By replacing the single wiggly line with the double wiggly line, Fig. 1(a) becomes Fig. 1(e), which now incorporates all higher order diagrams similar as Fig. 1(c). With this substitution, we can now release the constraint of $\alpha \neq \beta$. Setting $\alpha = \beta$ in Fig. 1(c) does not violate any feynmann rule we used above, and it corresponds exactly to the diagram with the disconnected four-point correlation function in Eq. (9). In fact, one can easily notice that only the crossing term, *i.e.* the last term of Eq. (9), leads to a connected diagram of $G_{\alpha\beta}^{\omega}$, which is same as what we derived in Eq. (10), but with $\alpha = \beta$.

Repeating the above procedure, one could, in principle, calculate all expansion terms, which contain the local complete vertices at one-, two-, ..., n-particle levels. The one-particle Green's function calculated in Eq. (4) is then dressed by these local scattering processes. It is easy to see that the non-locality is generated from the non-local coupling of these local scattering modes. The more terms are considered in the expansion, the better approximation of $G_{\alpha\beta}^{\omega}$ will be obtained. However, for practical reason, it is not possible to consider all expan-

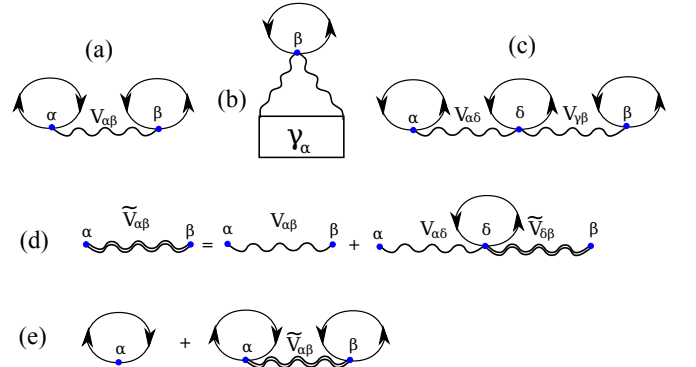


FIG. 1. A few lowest order Feynmann diagrams in the expansion of Eq. (4). (a), (b) and (c) correspond to the first three expansions. (d) The local single-particle charge fluctuations renormalize the non-local hybridization. With the renormalized hybridization $\tilde{V}_{\alpha\beta}$, diagrams similar to (a) and (c) now can be simply written as (e).

sion terms. A truncation of the expansion has to be done. As all expansion terms contribute to the calculation of $G_{\alpha\beta}^{\omega}$ in Eq. (4), there is no principle to favour certain terms over the others in the expansion. As we will see in the next section, however, a simple truncation of the expansion at certain order will violate some exact limit of the problem. Only by summing certain similar diagrams up to the infinite order, one can reproduce these limits. In the next section, we will examine one truncation scheme (more precisely, one diagram resummation scheme), which respects these exact limits and is feasible for practical implementation.

B. diagram resummation

First, we show that the inclusion of all diagrams similar to Fig. 1(a) and (c) is of crucial importance to our non-local expansion scheme. It has a very crucial implication in the non-interacting limit. With the dressed hybridization in Eq. (11), Fig. 1(a), (c) and all other similar diagrams can be cast into one simple diagram shown as Fig. 1(e). The single-particle Green's function evaluated from this diagram is given as:

$$G_{\alpha\beta}^{\omega,(e)} = g_{\alpha}^{\omega}\delta_{\alpha,\beta} + g_{\alpha}^{\omega}\tilde{V}_{\alpha\beta}^{\omega}g_{\beta}^{\omega}. \quad (12)$$

In the following, we will show that, with the dressed hybridization, Eq. (12) gives rise to $G_{\alpha\beta}^{0,\omega}$ exactly. This is a crucial condition to fulfill, as the non-interacting limit is an intuitive case to verify a diagrammatic approach. When interaction is switched off, *i.e.* $U = 0$, all reducible multi-particle susceptibilities vanish, thus, the only diagram we need to evaluate is Fig. 1(e).

$$G_{\alpha\beta}^{\omega} = g_{\alpha}^{0,\omega}\delta_{\alpha\beta} + g_{\alpha}^{0,\omega}[V^{-1} - g^0]_{\alpha\beta}^{-1}g_{\beta}^{0,\omega}. \quad (13)$$

In this equation, g_{α}^0 is the local single-particle Green's function in the non-interacting limit, which shall be understood as $[[\mathcal{G}_{\sigma}(\omega)]_{\alpha\alpha}^{-1}]^{-1}$. It is different from the local Weiss field $\mathcal{G}_{\alpha\alpha}(\omega)$.

$$\begin{aligned} G_{\alpha\beta}^{\omega} &= g_{\alpha}^{0,\omega}\delta_{\alpha\beta} + g_{\alpha}^{0,\omega} \left[\frac{Vg^0}{\mathbb{1} - Vg^0} \right]_{\alpha\beta} \\ &= g_{\alpha}^{0,\omega}\delta_{\alpha\beta} - g_{\alpha}^{0,\omega} \left[\mathbb{1} - \frac{\mathbb{1}}{\mathbb{1} - Vg^0} \right]_{\alpha\beta} \\ &= \left[\frac{\mathbb{1}}{g^{0,-1}\mathbb{1} - V} \right]_{\alpha\beta} = \mathcal{G}_{\alpha\beta}^{\omega}. \end{aligned} \quad (14)$$

Thus, the inclusion of local one-particle charge fluctuations at different spatial locations under the coupling of non-local hybridizations gives rise to the exact dynamics at all length scales in the non-interacting limit. At this point, it shall also be mentioned that, the current scheme can also correctly describe the strong coupling limit. In the strong coupling limit, the local dynamics become dominant, the expansion over $V_{\alpha\beta}$ becomes less important. \mathcal{S}_{loc} accounts for the major dynamics in that case.

In the intermediate coupling region, the diagrams with vertices become relevant. One example is Fig. 1(b), and more similar diagrams appear in the higher order expansions of Eq. (4). In these diagrams, similar to the renormalization of the hybridization shown in Eq. (11), the higher order terms can be viewed as the dressed diagrams of lower order terms. Thus, we can cast these diagrams into a more compact form by using these lower-order diagrams as building blocks. Certainly, there are different ways to construct the higher-order diagrams from these building blocks, which corresponds to the different choices of the subset of the complete Feynmann diagrams in the expansion of Eq. (4). In this work, we consider

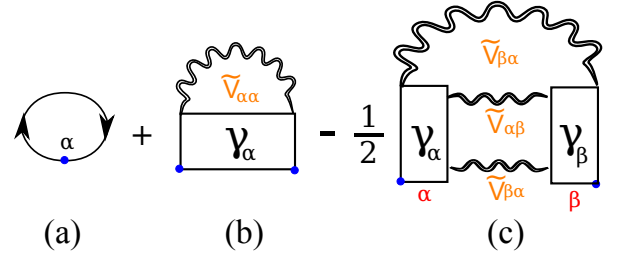


FIG. 2. The one-particle irreducible diagrams $\Lambda_{\alpha\beta}^{\omega}$ used for constructing the connected lattice Green's function in the non-local expansion scheme.

the following resummation scheme whose physics meaning becomes clear in the end of this section.

$$G_{\alpha\beta}^{\omega} = \left[\frac{\Lambda_{\alpha\beta}^{\omega}}{\mathbb{1} - V\omega\Lambda^{\omega}} \right]_{\alpha\beta}, \quad (15)$$

in which $\Lambda_{\alpha\beta}^{\omega}$ is the one-particle fully irreducible (1PI) diagrams taken as the construction blocks. Eq. (15) connects different 1PI diagrams of the single-particle propagator by the bare hybridization $V_{\alpha\beta}^{\omega}$. Intuitively, in Eq. (15), if we take the simplest 1PI diagram, which is $g_{\alpha\beta}^{\omega}\delta_{\alpha\beta}$, Eq. (12) is reproduced. It is obvious that, the more 1PI diagrams are adopted in $\Lambda_{\alpha\beta}^{\omega}$, the better approximation we can get for $G_{\alpha\beta}^{\omega}$. As one will see in the next section, Eq. (15) can reproduce one advanced many-body approach, *i.e.* dual-fermion approach [24], when the local system is taken as the DMFT impurity.

In these building block diagrams, not only the two-particle vertices but also higher-order vertices will appear. For practical reasons, we restrict our calculations to the two-particle vertices. It shall be noted here that, in addition to Eq. (15), one can also formulate other ways of summing diagrams with vertices. For simplicity, in this work we consider the 1PI diagrams Fig. 2 for $\Lambda_{\alpha\beta}^{\omega}$. The first diagram in Fig. 2 is the local single particle propagator $g_{\alpha\beta}^{\omega}\delta_{\alpha\beta}$ calculated from the local \mathcal{S}_{α} . This diagram only gives rise to a mean-field description of the inter-site Green's function, which equivalently means that the self-energy computed from this diagram is still local. This can be seen by starting from Eq. (12) and repeating the derivation in Eq. (14) with $g_{\alpha}^{-1} = g_{\alpha}^{0,-1} - \Sigma_{\alpha}$. One can easily see that the lattice self-energy function $\Sigma_{\alpha,\beta} = \Sigma_{\alpha}\delta_{\alpha,\beta}$ is exactly the same as the local self-energy obtained from \mathcal{S}_{α} , *i.e.* no non-locality is included in the self-energy. Fig. 2(b) corresponds to the diagrams with single-particle charge fluctuations coupled to local two-particle scattering modes, which is obtained from Fig. 1(b) by replacing the hybridization with the dressed one, see Eq. (11). It is crucial to note that, though this diagram is local in space, through Eq. (15), it generates spatial dependence of the *self-energy function* that is missing in Fig. 2(a). Fig. 2(c) consists of two connected four-point correlation functions $\gamma_{\alpha}^{\sigma_1\sigma_2;\sigma_3\sigma_4} = \langle c_{\alpha\omega_1}c_{\alpha\omega_2}^*c_{\alpha\omega_3}c_{\alpha\omega_4}^* \rangle_c$. In addition to the second diagram, it generates further non-local corrections to

the lattice self-energy. The sum of the internal spin indices involved in this diagram can be more conveniently carried out by introducing $\gamma_\alpha^{c/s} = \gamma_\alpha^{\uparrow\uparrow\uparrow\uparrow} \pm \gamma_\alpha^{\uparrow\uparrow\downarrow\downarrow}$. $\Lambda_{\alpha\beta}^\omega$ is then found to be:

$$\begin{aligned} \Lambda_{\alpha\beta}^\omega &= g_{\alpha\beta}^\omega \delta_{\alpha\beta} - T \sum_2 \gamma_\alpha^{\sigma_1\sigma_1;\sigma_2\sigma_2}(11;22) \tilde{V}_{\alpha\alpha}(\omega_2) \\ &\quad - \frac{T^2}{4} \sum_{234} \tilde{V}_{\beta\alpha}(\omega_2) \tilde{V}_{\beta\alpha}(\omega_4) \tilde{V}_{\alpha\beta}(\omega_3) \\ &\quad [3\gamma_\alpha^s(12;34)\gamma_\beta^s(43;21) + \gamma_\alpha^c(12;34)\gamma_\beta^c(43;21)] \end{aligned} \quad (16)$$

Here a compact form of frequency index is used, $1 \equiv (\omega_1, \sigma_1)$. The energy conservation requires $\omega_1 + \omega_3 = \omega_2 + \omega_4$ in the above equation.

Eq. (15) and Eq. (16) are the main results of our non-local expansion scheme. To construct non-locality from Eq. (16), only the local single-particle Green's function g_α^ω and the connected four-point correlation function $\gamma_\alpha^{c/s}(12;34)$ are required. They are obtained from the solution of the local problem defined by \mathcal{S}_α , which can be solved with modern numerical algorithms. Thus, the total number of correlated sites N in these equations can be reasonably large to represent the thermodynamic limit. In this sense, both the short- and the long-range spatial fluctuations can be described by this formalism.

The computation flow of this new scheme is the following: one starts with the construction of the Weiss field $\mathcal{G}_{\alpha\beta}^\omega$ and separates the local and non-local components as shown in Eq. (3). The local problem defined by the local component $\mathcal{G}_{\alpha\alpha}^\omega$ and μ_α , U_α is then solved to get the local single-particle Green's function g_α^ω and the connected four-point correlation function $\gamma_\alpha^{c/s}(12;34)$. Now Eq. (16) can be issued to compute the Green's functions $\Lambda_{\alpha\beta}^\omega$, which contain the non-trivial spatial fluctuations. With the new Green's function $G_{\alpha\beta}^\omega$ from Eq. (15), the self-energy $\Sigma_{\alpha\beta}^\omega$ can be calculated from Dyson equation, which contains both the local and non-local components and serves as the input for the next iteration of this calculation. The entire calculation shall stop only when $\Sigma_{\alpha\beta}^\omega$ does not change anymore.

The current scheme is formulated for the correlated system without translational symmetry. But it also applies to systems characterized by the quantum number k . As one unified scheme for both cases, here we also present the corresponding formula for the latter case. When the system is translationally invariant, only one impurity problem needs to be solved. The local impurity correlation functions g^ω and $\gamma^{s/c}$ become completely site independent. After applying Fourier transformation to Eq. (15) and Eq. (16), we have the following expressions for the lattice Green's function from the non-local

expansion scheme:

$$\begin{aligned} G_k^\omega &= \Lambda_k^\omega / [1 - V_k^\omega \Lambda_k^\omega], \\ \Lambda_k^\omega &= g^\omega - T \sum_2 \gamma_\alpha^{\sigma_1\sigma_1;\sigma_2\sigma_2}(11;22) \tilde{V}_{\alpha\alpha}(\omega_2) \\ &\quad - \frac{T^2}{4N^2} \sum_{234} \sum_{k',q} \tilde{V}_{k+q}(\omega_2) \tilde{V}_{k'}(\omega_4) \tilde{V}_{k'+q}(\omega_3) \\ &\quad [3\gamma^s(12;34)\gamma^s(43;21) + \gamma^c(12;34)\gamma^c(43;21)]. \end{aligned} \quad (17a)$$

Before closing this section, we want to further comment on the diagram resummation scheme. It shall be noted that such a scheme is not unique. Beside the free choice on the local limit, it is another feature of our non-local expansion method that different diagram resummation schemes are allowed. For simplicity, in Eq. (15) we only considered diagrams with one- and two-particle vertices. But there is no problem to include higher-order vertices in $\Lambda_{\alpha\beta}^\omega$. Other choices of the lower-order building-block diagrams as well as different ways of constructing higher-order reducible diagrams are possible. The only constraint on the building-block diagrams is to require them to be 1PI, otherwise some diagrams will be duplicated after the resummation. As an example to illustrate such feasibility, we present another resummation scheme in Fig. 3.

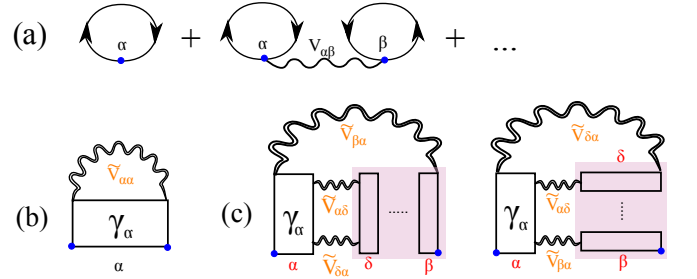


FIG. 3. Another set of building-block diagrams and the corresponding resummation scheme, which are different from those shown in Fig. 2. The diagrams inside the pink box represents a sum of all ladder diagrams with the two-particle vertices.

Fig. 3 contains only the one- and two-particle vertices, in this sense it is similar to Fig. 2. But it contains essentially different diagrams and represents a different resummation scheme. Here we sum the diagrams in Fig. 3(a) up to infinite order. One can find the corresponding expression for Fig. 3(a) in Eq. (14). Fig. 3(b) is same as Fig. 2(b), which is the lowest diagram concerning two-particle vertex. The diagram resummation in Fig. 3(c) is more subtle. Here we do not use the entire Fig. 3(c) as building-block diagram, but consider the sum of the local two-particle vertices in a ladder, which is graphically shown in the pink box in Fig. 3(c). Mathematically, this

sum is known as the Bethe-Salpeter equation.

$$\Gamma_{\alpha\beta}^{c/s}(12;34) = \gamma_{\alpha}^{c/s}(12;34)\delta_{\alpha\beta} - T \sum_{\delta=1}^N \sum_{5,6} \gamma_{\alpha}^{c/s}(12;56) \tilde{V}_{\delta\alpha}(\omega_5) \tilde{V}_{\alpha\delta}(\omega_6) \Gamma_{\delta\beta}^{c/s}(65;34) \quad (18)$$

From this equation, one can easily understand that, after summing all ladder diagrams, the resulting dressed two-particle vertex $\Gamma_{\alpha\beta}^{c/s}$ becomes non-local. As shown in Fig. 3(c), the dressed two-particle vertices from both the particle-hole horizontal and vertical channels are then used to construct the one-particle Green's function. A compact expression for Fig. 3(c) can be obtained by employing the crossing relation of $\Gamma_{\alpha\beta}^{c/s}$ in the horizontal and vertical channels, as well as the crossing symmetry of $\gamma_{\alpha}^{c/s}$. The expression for Fig. 3 is in the end found to be:

$$\begin{aligned} G_{\alpha\beta}^{\omega} &= \left[\frac{\mathbb{1}}{g^{0,-1}\mathbb{1} - V} \right]_{\alpha\beta} \\ &- T \sum_2 \gamma_{\alpha}^{\sigma_1\sigma_1;\sigma_2\sigma_2}(11;22) \tilde{V}_{\alpha\alpha}(\omega_2) \\ &- \frac{T^2}{2} \sum_{\delta=1}^N \sum_{234} \tilde{V}_{\beta\alpha}(\omega_2) \tilde{V}_{\alpha\delta}(\omega_3) \tilde{V}_{\delta\alpha}(\omega_4) \\ &\left\{ \gamma_{\alpha}^c(12;34) [\Gamma_{\delta\beta}^c(43;21) - \frac{1}{2}\gamma_{\beta}^c(43;21)] \right. \\ &\left. + 3\gamma_{\alpha}^s(12;34) [\Gamma_{\delta\beta}^s(43;21) - \frac{1}{2}\gamma_{\beta}^s(43;21)] \right\}. \end{aligned} \quad (19)$$

III. APPLICATION: NEW INSIGHTS INTO THE DUAL-FERMION APPROACH

The non-local expansion scheme corresponds to the linked-cluster (or cumulant) expansion approach [6, 8, 32, 33] if V_{ij} is simply taken as t_{ij} in Eq. (1) and all terms in Eq. (4) are considered (thus, no diagram resummation is required.). The diagram-resummation algorithm in Eq. (15) corresponds to the scheme discussed in Refs. 34 and 35. As discussed before, the choice of local system is quite flexible in the non-local expansion scheme. In the following section, we will show that, by choosing a different local limit, the current scheme can be connected to and further extend some well-known local many-body approaches. As the first application, we will show that the DF approach exactly corresponds to one special case of the non-local expansion scheme for a translationally invariant system. From the current non-local expansion scheme, we want to explain the physics hidden behind the usage of the dual variables.

In Eq. (4), we have employed a direct expansion of V_{ij} and considered the expansion in orders. Now, we want to perform the same expansion by introducing a dual variable through the Hubbard-Stratonovich transformation. This is also known as a strong-coupling expansion of the Hubbard model [5, 36]. The main question we

want to address in this section is that, by taking a different form of V_{ij} , we can prove that the dual-fermion approach [24] is equivalent to the current non-local expansion scheme with the diagram resummation algorithm shown in Eq. (17).

The DF approach is an elegant non-local extension of the DMFT, which was proposed for systems with translational symmetry. However, there is obvious no obstacle for it to apply to inhomogeneous systems. One only needs to be careful with the breaking of translational symmetry and formulate it in coordination, instead of momentum space. Here, we would instead use Eq. (17) and prove that the current scheme can reproduce the DF approach for a translationally invariant system, if the local action is taken as the DMFT one.

According to the DF approach, we add and subtract a local dynamic function $\Delta_i(\omega)$ to Eq. (3),

$$\begin{aligned} S &= \sum_{i=1}^N \mathcal{S}_i + T \sum_{i,j} c_{i\omega}^* [\mathcal{G}_{\sigma}^{-1}(\omega)]_{ij} c_{j\omega} \\ &= \sum_{i=1}^N \mathcal{S}_i - T \sum_{k,\omega} c_{k\omega}^* (\Delta_{\omega} - \epsilon_k) c_{k\omega}, \end{aligned} \quad (20)$$

where \mathcal{S}_i is the local action of the impurity at the i th site, $\mathcal{S}_i = -(\omega + \mu) + \Delta_{\omega} + U n_{i\uparrow} n_{i\downarrow}$. Δ_{ω} , in principle, can be an arbitrary function. As shown in the dual fermion approach, diagrams for the DF self-energy can be simplified if Δ_{ω} is taken as the hybridization function of the DMFT. In Eq. (20), V_k^{ω} is given as $-(\Delta_{\omega} - \epsilon_k)$, which contains both local and non-local components. One can still repeat the procedure shown in Sec. II to calculate the non-local single-particle Green's function. Due to the inclusion of the local component in V_k^{ω} , there are additional diagrams which shall be considered. Fortunately, such diagrams, after the renormalization of V_k^{ω} , have actually been included in Fig. 2. Thus, the final expression of the single-particle Green's function from the non-local expansion scheme Eq. (17), also applies to the current case.

In the following, we want to show two important observations of the DF approach. *First, we show that the physics origin of the non-interacting DF propagator corresponds exactly to the renormalized hybridization \tilde{V}_k^{ω} .* To see this, we need to slightly modify the construction of the DF approach. Different from the Hubbard-Stratonovich transformation generally employed in the dual fermion approach [24], we set the coefficient of the mixing term between the original and the dual variables to be one. The full action in Eq. (20) becomes

$$\begin{aligned} \mathcal{S} &= \mathcal{S}[c^*, c; f^*, f] = \sum_{i=1}^N \mathcal{S}_i - \\ &- T \sum_{k,\omega} [f_{k\omega}^* c_{k\omega} + c_{k\omega}^* f_{k\omega} + \frac{f_{k\omega}^* f_{k\omega}}{\Delta_{\omega} - \epsilon_k}]. \end{aligned} \quad (21)$$

Then we proceed in the same way as the normal DF approach [24] does to get the exact relation between the

lattice Green's function and the so-called DF Green's function:

$$G_{\alpha\beta}^{\omega} = (\Delta_{\omega} - \epsilon_k)^{-1} + (\Delta_{\omega} - \epsilon_k)^{-1} G_k^{d,\omega} (\Delta_{\omega} - \epsilon_k)^{-1}, \quad (22)$$

where $G_k^{d,\omega}$ is the single-particle propagator defined for the dual variables, whose non-interacting part is given as:

$$G_k^{d,0,\omega} = -[(\Delta_{\omega} - \epsilon_k)^{-1} + g^{\omega}]^{-1} = \tilde{V}_k^{\omega}. \quad (23)$$

From Eq. (23), one immediately understands that the non-interacting dual fermion propagator is not just a mathematical definition, it has clear physical correspondence. It corresponds to the dressed hybridization we obtained in Eq. (11). As shown in the DF approach [24], the coarse graining of $G_k^{d,0,\omega}$ corresponds to the DMFT self-consistent equation.

$$-\sum_k \frac{1}{(\Delta_{\omega} - \epsilon_k)^{-1} + g^{\omega}} = \sum_k \tilde{V}_k^{\omega} = 0, \quad (24)$$

which indicates that the average of the non-local hybridization \tilde{V}_k^{ω} in momentum space is zero. This, from another perspective, reveals the local nature of the DMFT, *i.e.* the coarse graining effect of the non-local fluctuations vanishes in the single-particle level.

It also becomes transparent now that, in the non-interacting limit for the dual variables, the DF approach can give rise to the correct weak-coupling and the strong-coupling behaviors for a reason exactly the same as we discussed in Eq. (14). Furthermore, Eq. (23) also implies that the self-energy in the DF approach has the same set of Feynmann diagrams as the Green's function in our non-local expansion scheme, *i.e.* Fig. 2(b) and (c) are also the first two diagrams for the self-energy in the DF approach. As the DF self-energy is known to be analytic [24], the lattice Green's function of the non-local expansion scheme is, therefore, also an analytic function.

What is more subtle about the DF approach, which is the second important observation of this section, is that *it exactly the same as our non-local expansion scheme with the diagram-resummation algorithm Eq. (17)*. To prove this, we show the equivalence of Eq. (22) to Eq. (17). Starting from Eq. (22), after substituting $G_k^{d,\omega}$ with $G_k^{d,0,\omega}$ and the DF self-energy $\Sigma_k^{d,\omega}$, we have

$$\begin{aligned} G_k^{\omega} &= (\Delta_{\omega} - \epsilon_k)^{-1} + \frac{(\tilde{V}_k^{\omega,-1} - \Sigma_k^{d,\omega})^{-1}}{(\Delta_{\omega} - \epsilon_k)^2} \\ &= -\frac{1}{V_k^{\omega}} + \frac{(\tilde{V}_k^{\omega,-1} - \Sigma_k^{d,\omega})^{-1}}{(V_k^{\omega})^2} \\ &= -\frac{1}{V_k^{\omega}} + \frac{1}{(V_k^{\omega})^2} \frac{V_k^{\omega}/(1 - V_k^{\omega} g^{\omega})}{1 - V_k^{\omega} \Sigma_k^{d,\omega}/(1 - V_k^{\omega} g^{\omega})} \\ &= -\frac{1}{V_k^{\omega}} \left[1 - \frac{1}{1 - V_k^{\omega} (g^{\omega} + \Sigma_k^{d,\omega})} \right] \\ &= \frac{g^{\omega} + \Sigma_k^{d,\omega}}{1 - V_k^{\omega} (g^{\omega} + \Sigma_k^{d,\omega})}. \end{aligned} \quad (25)$$

In the above derivation, Eq. (11) and Eq. (23) have been employed. As we discussed before, the first two DF self-energy function employs the same Feynmann diagrams as shown in Fig. 2(b) and (c), *i.e.* $g^{\omega} + \Sigma_k^{d,\omega} = \Lambda_k^{\omega}$. Thus, Eq. (25) is exactly the same as Eq. (17). As no dual variable is involved in the construction of the non-local expansion scheme, the dynamics and physical correspondence of each term in Eq. (17) is clear. The equivalence of the DF and the non-local expansion scheme, thus, indicates that the interacting nature of the lattice fermions in the DF approach with the first two self-energy diagrams is given exactly by Fig. 2, in which three different processes are taken as the most important contributions to the dynamics at all length scales. The first one reproduces the non-interacting limit through the non-local charge fluctuations; the non-local corrections to the lattice self-energy are approximated by a single two-particle-scattering mode in Fig. 2(b) and the coupling of two two-particle-scattering processes in Fig. 2(c). All three processes, then, are coupled through Eq. (15) by the non-local hybridization V_k^{ω} . Such picture is less obvious in the DF approach.

Based on the equivalence of Eq. (25) and Eq. (17), it is no surprise that the lattice self-energy of the non-local expansion scheme is same as that of the DF approach. With Eq. (17), the lattice self-energy is found to be:

$$\begin{aligned} \Sigma_k^{\omega} &= \omega + \mu - \epsilon_k - 1/G_k^{\omega} \\ &= \omega + \mu - \epsilon_k - (g^{\omega} + \Sigma_k^{d,\omega}) + V_k^{\omega} \\ &= \omega + \mu - \Delta_{\omega} - 1/(g^{\omega} + \Sigma_k^{d,\omega}). \end{aligned} \quad (26)$$

Given the DMFT Dyson equation $g^{\omega,-1} = \omega + \mu - \Delta_{\omega} - \Sigma_{loc}^{\omega}$, the above equation is then simplified as

$$\begin{aligned} \Sigma_k^{\omega} &= \Sigma_{loc}^{\omega} + 1/g^{\omega} - 1/(g^{\omega} + \Sigma_k^{d,\omega}) \\ &= \Sigma_{loc}^{\omega} + \frac{\Sigma_k^{d,\omega}}{g^{\omega} (g^{\omega} + \Sigma_k^{d,\omega})} \\ &= \Sigma_{loc}^{\omega} + \frac{\Sigma_k^{d,\omega}/(g^{\omega})^2}{1 + g^{\omega} \Sigma_k^{d,\omega}/(g^{\omega})^2}. \end{aligned} \quad (27)$$

This is exactly same as Eq. (18) of Ref. 37.

In the last part of this section, we present a calculation for a correlated system with translational symmetry by using the non-local expansion scheme Eq. (17), which also represents a solution of the DF approach. In order to fully demonstrate the non-locality generated by these two approaches, we show, in Fig. 4, the lattice self-energy for a three dimensional cubic lattice with $U/t = 8$ along the high symmetry line R-M-X-Γ-R. Results from large cluster DCA calculations [39] with the same parameters are available for comparison. The DMFT solutions have no momentum dependence, thus, they are straight lines in Fig. 4. The inclusion of non-locality, as shown in Eq. (17), generates dispersion in the real- and imaginary-part of the lattice self-energy around the DMFT solutions. Here, results are shown for two different temperatures. The lower temperature ($\beta t = 2.6$, see

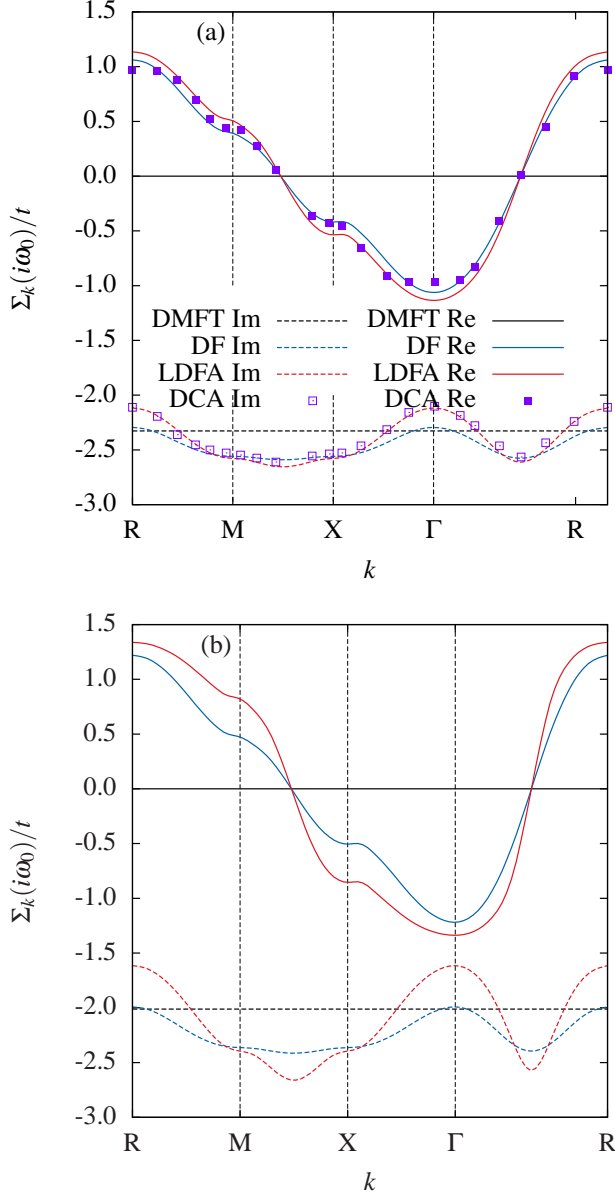


FIG. 4. The momentum dependence of the lattice self-energy in the non-local expansion scheme, as well as in the DF approach, for the single-band Hubbard model on a cubic lattice at (a) $\beta t = 2$, (b) $\beta t = 2.6$ and $U/t = 8$. The solid and dashed lines correspond to the real and imaginary parts of Σ_k^ω at the lowest Matsubara frequency. They agree well with the results from a calculation within DCA with a 100 site cluster [38] which are replotted as squares here.

Fig. 4(b)) results display more pronounced momentum dependence of $\Sigma_k(i\omega_0)$ than the higher temperature ($\beta t = 2.0$, see Fig. 4(a)) ones. With the decrease of temperature, the spatial fluctuations are enhanced. In addition to the results from the DF approach and the non-local expansion scheme, Fig. 4 also shows the corresponding solution from Eq. (17) with a modified Λ_k^ω . In addition to the diagrams shown in Fig. 2, all ladder-type

diagrams in the both horizontal and vertical channels are included in this calculation. The additional scattering processes included in the ladder diagrams yields a better inclusion of non-locality, thus, a more pronounced momentum dependence of $\Sigma_k(i\omega)$ can be observed. Without overhead thinking, one can immediately understand that the adoption of the ladder diagrams in Λ_k^ω (which can be generated by replacing γ_β in Fig. 2 by the corresponding ladders $\Gamma_{\delta\beta}$) in the non-local expansion scheme corresponds exactly to the ladder dual fermion approach (LDFA) [26]. We want to note that the LDFA results show surprisingly good agreement (especially the imaginary part) with the one from a DCA calculations with a cluster of 100 sites (see Fig. 5 in Ref. 39). Compared to the time-consuming large cluster DCA calculations, the present non-local expansion scheme, as well as the DF approach, is numerically much more economical. Note, in the DCA⁺ scheme [38] proposed recently, a continuous lattice self-energy can also be achieved with much less numerical effort, which represents another promising route to understand the non-locality of a quantum many-body system.

IV. OUTLOOK

Besides the intuitive understanding of the DF approach, in this section, we want to briefly outlook other possible applications of the non-local expansion scheme. More detailed discussions and the corresponding results will be presented elsewhere.

First, we want to show that the non-local expansion scheme can be used as a quick cluster solver for the Cellular-DMFT. In the Cellular-DMFT, the translational symmetry is naturally broken due to the different intra- and inter-cluster hopping amplitudes. Though in some special cases (for example in a 2x2 square cluster), the cluster momenta are still a good quantum number, we usually have to work with the situation that translational invariance is lost. Thus, Eq. (15) and (16) shall be used. In the Cellular-DMFT, the Weiss field contains the inter- and intra-cluster components. For a calculation with the non-local expansion scheme, in the first step we only need the diagonal component of the hybridization function $\Delta_{i,i}^\omega$, which we adopt to construct the local Weiss field $\mathcal{G}_i^\omega = -1/(\omega + \mu - \Delta_{i,i}^\omega)$, which is different from the diagonal component of the Weiss field from the cellular-DMFT $\mathcal{G}_{i,i}^\omega = -[(\omega + \mu)\mathbb{1} - \Delta]_{i,i}^{-1}$. Thus, the separation of the local and non-local degrees of freedom looks like:

$$\mathcal{S} = \sum_{i=1}^N \mathcal{S}_i - T \sum_{i \neq j} \sum_{\omega} c_{i\omega\sigma}^* \Delta_{i,j}^\omega c_{j\omega\sigma}. \quad (28)$$

With the new \mathcal{G}_i^ω , an interacting impurity problem defined by \mathcal{S}_i is then solved to get the local self-energy Σ_i^ω and the local single-particle propagator g_i^ω , as well as the connected four-point correlation function $\gamma_i^{s/c}$. In

the second step, the non-local expansion scheme Eq. (15) will be issued to calculate both the local and non-local components of the single-particle propagator g_{ij}^ω and the self-energy function $\Sigma_{i,j}^\omega$. The new Weiss field then can be calculated from $\Sigma_{i,j}^\omega$, which closes the Cellular-DMFT self-consistency loop. As one can immediately understand, the application of the non-local expansion scheme to the Cellular-DMFT equations can reduce the computational effort of solving a cluster problem to that of solving an impurity problem. Thus, a larger cluster calculation can be expected for the Cellular-DMFT with the non-local expansion scheme as cluster solver.

Second, the non-local expansion scheme can extend the R-DMFT to incorporate non-locality in the self-energy function. R-DMFT is widely used in the study of disordered correlated systems [40–44]. The disorders we considered here can be the different site energies ϵ_i and electronic correlations U_i , which are local in space. Thus, a DMFT-fashion calculation can be formulated. The R-DMFT iteration cycle begins with the calculation of the lattice Green's function,

$$G_{i,j}^\omega = \left[\frac{1}{(\omega + \mu)\mathbb{1} - \hat{t} - \hat{\epsilon} - \Sigma^\omega} \right]_{i,j}, \quad (29)$$

in which \hat{t} and $\hat{\epsilon}$ are of matrix forms. Matrix Σ^ω , in R-DMFT, is simplified to have only diagonal elements Σ_i^ω . For each site i , one defines a Weiss field $\mathcal{G}_i^\omega = [G_{i,i}^{\omega,-1} + \Sigma_i^\omega]^{-1} = (\omega + \mu) - \epsilon_i - \Delta_i^\omega$, from which the local Green's function g_i^ω and a new local self-energy Σ_i^ω can be calculated in the conventional DMFT. Normally, the R-DMFT closes the iteration cycle by substituting the new Σ_i^ω to Eq. (29). Now, with the non-local expansion scheme, a non-local self-energy can be obtained for the R-DMFT. Like in the DF approach, we separate the local and non-local degrees of freedom by adding and subtracting a local dynamic function Δ_i^ω to the denominator of Eq. (29). The non-local hybridization used for expansion in the non-local expansion scheme can be easily identified as $-(\Delta_i^\omega\mathbb{1} - \hat{t})$. With Eq. (15), a self-energy matrix with off-diagonal elements can be obtained, which generates the non-trivial spatial fluctuations to the R-

DMFT. Here, it has to be noted that at each site i , g_i^ω and $\gamma_i^{c/s}$ take different values due to the site-dependent disorders. Thus, the single-particle charge fluctuations and the two-particle scattering modes differ at different sites. For this reason, the non-local expansion scheme essentially extends the non-local correlations of the R-DMFT from the one-particle to the two-particle level.

V. CONCLUSIONS

In this paper, we proposed a non-local expansion scheme to study correlated many-fermion systems. By separating the local and non-local degrees of freedom and assuming that the local system can be solved exactly (which, at least, can be achieved numerically), we can treat the non-local terms as a small perturbation to the local degrees of freedom. A non-local expansion around the solution of the local system can generate, order by order, the non-local corrections to the local solutions. This scheme can be widely applied to correlated systems with/without translational symmetry. Numerically, it is as economical as the DMFT, thus, a continuous momentum dependence in the self-energy function can be achieved easily in this scheme. As the first application, we have proven that the DF approach can be beautifully explained as one special case of the non-local expansion scheme presented in this work. When the local system is taken as the DMFT impurity and Λ_k^ω is approximated as the diagrams shown in Fig. 2 or ladder-type diagrams, the DF or the LDFA can be reproduced.

ACKNOWLEDGMENTS

We thank A.N. Rubtsov, H. Lee, H. Monien, H. Hafermann, A.I. Lichtenstein and W. Hanke for the fruitful collaborations on the dual-fermion approach. We thank A. Fleszar, K.S. Chen and Tin Ribic for reading the manuscript. We acknowledge the support from the DFG Grants No. Ha 1537/23-1 within the Forschergruppe FOR 1162 and SPP Ha 1537/24-2.

-
- [1] Felix Bloch, “über die quantenmechanik der elektronen in kristallgittern,” *Zeitschrift für Physik* **52**, 555–600 (1929).
 - [2] P. W. Anderson, “Absence of diffusion in certain random lattices,” *Phys. Rev.* **109**, 1492–1505 (1958).
 - [3] Immanuel Bloch, Jean Dalibard, and Wilhelm Zwerger, “Many-body physics with ultracold gases,” *Rev. Mod. Phys.* **80**, 885–964 (2008).
 - [4] N. E. Bickers, D. J. Scalapino, and S. R. White, “Conserving approximations for strongly correlated electron systems: Bethe-salpeter equation and dynamics for the two-dimensional hubbard model,” *Phys. Rev. Lett.* **62**, 961–964 (1989).
 - [5] S K Sarker, “A new functional integral formalism for strongly correlated fermi systems,” *Journal of Physics C: Solid State Physics* **21**, L667 (1988).
 - [6] Walter Metzner, “Linked-cluster expansion around the atomic limit of the hubbard model,” *Phys. Rev. B* **43**, 8549–8563 (1991).
 - [7] N. DUPUIS and S. PAIRAULT, “A strong-coupling expansion for the hubbard model,” *International Journal of Modern Physics B* **14**, 2529–2560 (2000).
 - [8] Stéphane Pairault, David Sénéchal, and A.-M. S. Tremblay, “Strong-coupling expansion for the hubbard model,” *Phys. Rev. Lett.* **80**, 5389–5392 (1998).

- [9] R. Blankenbecler, D. J. Scalapino, and R. L. Sugar, "Monte carlo calculations of coupled boson-fermion systems. i," *Phys. Rev. D* **24**, 2278–2286 (1981).
- [10] D. J. Scalapino and R. L. Sugar, "Monte carlo calculations of coupled boson-fermion systems. ii," *Phys. Rev. B* **24**, 4295–4308 (1981).
- [11] Antoine Georges, Gabriel Kotliar, Werner Krauth, and Marcelo J. Rozenberg, "Dynamical mean-field theory of strongly correlated fermion systems and the limit of infinite dimensions," *Rev. Mod. Phys.* **68**, 13–125 (1996).
- [12] R. W. Helmes, T. A. Costi, and A. Rosch, "Mott transition of fermionic atoms in a three-dimensional optical trap," *Phys. Rev. Lett.* **100**, 056403 (2008).
- [13] A. Katanin, "Self-energy effects in the polchinski and wick-ordered renormalization-group approaches," *Journal of Physics A: Mathematical and Theoretical* **44**, 495004 (2011).
- [14] Thomas Maier, Mark Jarrell, Thomas Pruschke, and Matthias H. Hettler, "Quantum cluster theories," *Rev. Mod. Phys.* **77**, 1027–1080 (2005).
- [15] M. H. Hettler, M. Mukherjee, M. Jarrell, and H. R. Krishnamurthy, "Dynamical cluster approximation: Nonlocal dynamics of correlated electron systems," *Phys. Rev. B* **61**, 12739–12756 (2000).
- [16] M. Jarrell, Th. Maier, C. Huscroft, and S. Moukouri, "Quantum monte carlo algorithm for nonlocal corrections to the dynamical mean-field approximation," *Phys. Rev. B* **64**, 195130 (2001).
- [17] S. Moukouri, S. Allen, F. Lemay, B. Kyung, D. Poulin, Y. M. Vilks, and A.-M. S. Tremblay, "Many-body theory versus simulations for the pseudogap in the hubbard model," *Phys. Rev. B* **61**, 7887–7892 (2000).
- [18] S. Moukouri and M. Jarrell, "Absence of a slater transition in the two-dimensional hubbard model," *Phys. Rev. Lett.* **87**, 167010 (2001).
- [19] C. J. Bolech, S. S. Kancharla, and G. Kotliar, "Cellular dynamical mean-field theory for the one-dimensional extended hubbard model," *Phys. Rev. B* **67**, 075110 (2003).
- [20] Gabriel Kotliar, Sergej Y. Savrasov, Gunnar Pálsson, and Giulio Biroli, "Cellular dynamical mean field approach to strongly correlated systems," *Phys. Rev. Lett.* **87**, 186401 (2001).
- [21] Hiroaki Kusunose, "Influence of spatial correlations in strongly correlated electron systems: Extension to dynamical mean field approximation," *Journal of the Physical Society of Japan* **75**, 054713 (2006).
- [22] A. Toschi, A. A. Katanin, and K. Held, "Dynamical vertex approximation: A step beyond dynamical mean-field theory," *Phys. Rev. B* **75**, 045118 (2007).
- [23] Karsten Held, Andrey A. Katanin, and Alessandro Toschi, "Dynamical vertex approximation: An introduction," *Progress of Theoretical Physics Supplement* **176**, 117–133 (2008).
- [24] A. N. Rubtsov, M. I. Katsnelson, and A. I. Lichtenstein, "Dual fermion approach to nonlocal correlations in the hubbard model," *Phys. Rev. B* **77**, 033101 (2008).
- [25] S. Brener, H. Hafermann, A. N. Rubtsov, M. I. Katsnelson, and A. I. Lichtenstein, "Dual fermion approach to susceptibility of correlated lattice fermions," *Phys. Rev. B* **77**, 195105 (2008).
- [26] H. Hafermann, G. Li, A. N. Rubtsov, M. I. Katsnelson, A. I. Lichtenstein, and H. Monien, "Efficient perturbation theory for quantum lattice models," *Phys. Rev. Lett.* **102**, 206401 (2009).
- [27] G. Rohringer, A. Toschi, H. Hafermann, K. Held, V. I. Anisimov, and A. A. Katanin, "One-particle irreducible functional approach: A route to diagrammatic extensions of the dynamical mean-field theory," *Phys. Rev. B* **88**, 115112 (2013).
- [28] A. Valli, G. Sangiovanni, O. Gunnarsson, A. Toschi, and K. Held, "Dynamical vertex approximation for nanoscopic systems," *Phys. Rev. Lett.* **104**, 246402 (2010).
- [29] S.-X. Yang, P. Haase, H. Terletska, Z. Y. Meng, T. Pruschke, J. Moreno, and M. Jarrell, "Dual-fermion approach to interacting disordered fermion systems," *Phys. Rev. B* **89**, 195116 (2014).
- [30] J. Hubbard, "Calculation of partition functions," *Phys. Rev. Lett.* **3**, 77–78 (1959).
- [31] R. L. Stratonovich, "On a Method of Calculating Quantum Distribution Functions," *Soviet Physics Doklady* **2**, 416 (1957).
- [32] Andriy M. Shvaika, "Dynamical mean-field theory of correlated hopping: A rigorous local approach," *Phys. Rev. B* **67**, 075101 (2003).
- [33] Ehsan Khatami, Edward Perepelitsky, Marcos Rigol, and B. Sriram Shastry, "Linked-cluster expansion for the green's function of the infinite- u hubbard model," *Phys. Rev. E* **89**, 063301 (2014).
- [34] M.I. Vladimir and V.A. Moskalenko, "Diagram technique for the hubbard model," *Theoretical and Mathematical Physics* **82**, 301–308 (1990).
- [35] S.I. Vakar, M.I. Vladimir, and V.A. Moskalenko, "Diagram technique for the hubbard model. ii. metal-insulator transition," *Theoretical and Mathematical Physics* **85**, 1185–1192 (1990).
- [36] S. Pairault, D. Sñchal, and A.-M.S. Tremblay, "Strong-coupling perturbation theory of the hubbard model," *The European Physical Journal B - Condensed Matter and Complex Systems* **16**, 85–105 (2000).
- [37] A. N. Rubtsov, M. I. Katsnelson, A. I. Lichtenstein, and A. Georges, "Dual fermion approach to the two-dimensional hubbard model: Antiferromagnetic fluctuations and fermi arcs," *Phys. Rev. B* **79**, 045133 (2009).
- [38] Peter Staar, Thomas Maier, and Thomas C. Schulthess, "Dynamical cluster approximation with continuous lattice self-energy," *Phys. Rev. B* **88**, 115101 (2013).
- [39] Emanuel Gull, Peter Staar, Sebastian Fuchs, Phani Nukala, Michael S. Summers, Thomas Pruschke, Thomas C. Schulthess, and Thomas Maier, "Submatrix updates for the continuous-time auxiliary-field algorithm," *Phys. Rev. B* **83**, 075122 (2011).
- [40] V. Dobrosavljević and G. Kotliar, "Mean field theory of the mott-anderson transition," *Phys. Rev. Lett.* **78**, 3943–3946 (1997).
- [41] Yun Song, R. Wortis, and W. A. Atkinson, "Dynamical mean field study of the two-dimensional disordered hubbard model," *Phys. Rev. B* **77**, 054202 (2008).
- [42] D. Tanasković, V. Dobrosavljević, E. Abrahams, and G. Kotliar, "Disorder screening in strongly correlated systems," *Phys. Rev. Lett.* **91**, 066603 (2003).
- [43] E Miranda and V Dobrosavljevi, "Disorder-driven non-fermi liquid behaviour of correlated electrons," *Reports on Progress in Physics* **68**, 2337 (2005).
- [44] V. Dobrosavljević and E. Miranda, "Absence of conventional quantum phase transitions in itinerant systems with disorder," *Phys. Rev. Lett.* **94**, 187203 (2005).